Topology-optimized carpet cloaks based on a level-set boundary expression

Garuda Fujii*
Department of Mechanical Systems Engineering, Faculty of Engineering, Shinshu University, 4-17-1 Wakasato, Nagano 380-8553, Japan

Tsuyoshi Ueta
Physics Laboratory, The Jikei University School of Medicine, 8-3-1 Kokuryo-cho, Chofu, Tokyo 182-8570, Japan
(Received 24 June 2016; published 3 October 2016)

The concept of topology-optimized carpet cloaks is presented using level-set boundary expressions. Specifically, these carpet cloaks are designed with the idea of minimizing the value of an objective functional, which is here defined as the integrated intensity of the difference between the electric field reflected by a flat plane and that controlled by the carpet cloak. Made of dielectric material, our cloaks are designed to imitate reflections from a flat plane, and with some cloaks, the value of the objective functional falls below 0.12% of that for a bare bump on a flat plane. These optimal carpet cloaks spontaneously satisfy the time-reversal symmetry of the scattered field during the optimization process. The profiles associated with optimal configurations are controlled by adjusting a regularization parameter. With this approach, a variety of configurations with different structural characteristics can be obtained.

DOI: 10.1103/PhysRevE.94.043301

I. INTRODUCTION

Photonic crystals [1–3] and metamaterials [4] have been actively studied in recent years as a means to realize new functional devices to control light. Their structures determine function and performance of optical devices; various structures have been proposed such as periodic [1,2], random [5–7], fractal [8,9], amorphous [10], and others [11].

Carpet cloaks [12] have been proposed as an alternative means to realize optical invisibility [13,14] and to render an object on a flat plane invisible by imitating the reflections from a flat plane. To realize carpet cloaks, several unique structures, materials, and mechanisms have been proposed such as porous dielectric cloaks [15,16], woodpile photonic crystal-based carpet cloaks [17], and ultrathin carpet cloaks based on metasurfaces composed of closed ring resonators [18] and gold block-based nanoanntennas [19].

Topology optimization [20] is a structural methodology that exploits powerful numerical design algorithms to provide high-performance devices. It developed from the field of computational mechanics as researchers sought to address, for example, stiffness maximization problems [20,21]. Topology optimization has recently been applied to various design problems in engineering such as thermal diffusions [22], fluid dynamics [23], and acoustics [24]. Several optical devices have been designed for specific purposes using topology optimizations such as photonic crystals [25], photonic crystal cavities [26,27], photonic crystal-based flat lens [28], antireflective surfaces [29], waveguides [30], and metamaterials [31]. Optical cloaks have been designed using topology optimization based on density [32,33] and level-set [34–36] methods. The performances of the topology-optimized cloaks are evaluated numerically with the designed cloaks displaying an advanced cloaking performance not only in numerical simulations [37] but also in experiments [38]. The design and fabrication based on topology optimization is expected to be developed as another scheme different from that involving coordinate transformations [13,14], phase manipulations by metasurfaces [18,19], and scattering cancellation [39].

In this work, we apply topology optimization to the design of carpet cloaks and present carpet cloaks made of dielectrics with superior cloaking performances. The objective functional is defined as the integrated intensity of the difference between the electric field reflected by a flat plane and that controlled by a carpet cloak; carpet cloaks are designed to minimize the value of the objective functional. The profiles of the dielectric structures are expressed as level-set functions of piecewise-constant segments [40]; their dielectric boundaries are isosurfaces of these level-set functions [41]. Explicit expressions for the structural boundaries enable us to create computer-aided design data of optimal configurations having complex distributions of dielectrics and to fabricate the configurations precisely by using three-dimensional printers. Topology optimization of carpet cloaks is a strong multimodal problem and, in our numerical implementation, a specific initial configuration can be used to reach an optimal configuration having superior performance. Various optimal configurations can be obtained by adjusting a regularization parameter, and the presented topology optimization for our carpet cloaks is formulated using the notion of a fictitious interface energy [42].

II. OPTIMIZATION PROBLEM

Figure 1 shows a schematic of the topology optimization for the proposed carpet cloaks. A semicylindrical perfect-electric-conducting (PEC) bump, Ω_{PEC}, is set on a flat PEC reflector, represented by its boundary condition implemented on boundary Γ_{PEC}, and is concealed by a designed carpet cloak. The dielectric structure for the carpet cloak, Ω_{dm}, is designed and transformed into the design domain, Ω_{D}, for the purpose of enhancing its cloaking performance. The incident waves are assumed to be plane waves propagating at an incident angle of $\theta = \pi/4$. The finite-element (FE) method is used to analyze light scattering by the flat plane, the bump, and the dielectric carpet cloak. A perfectly matched layer (PML)

*g_fujii@shinshu-u.ac.jp

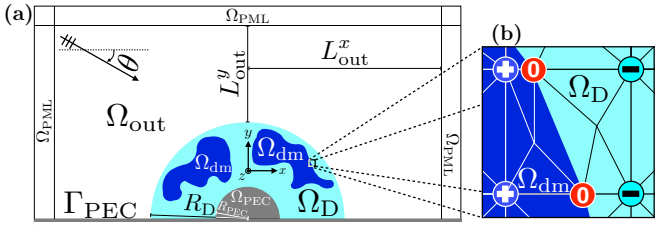

FIG. 1. Schematics of topology optimization for carpet cloaks and dielectric boundary interpreted as an isosurface of level-set functions. (a) For the carpet cloak structures, the domain sizes are $R_{\rm PEC} = R_{\rm D}/3$, $L^x_{\rm out} = 2R_{\rm D}$, $L^y_{\rm out} = R_{\rm D}$, and $L_{\rm grid} = R_{\rm D}/200$. (b) Level-set functions on grid points and a dielectric boundary obtained as the isosurface of these functions. Symbols "±" and "0" represent the signs of the level-set functions and the position at which level-set functions are linearly interpolated along grid lines become zero.

absorbing boundary condition [43] employing an optimized absorbing function [44] is used to simulate light scattered into the open regions; in the scheme, the PML is represented by $\Omega_{\rm PML}$. $\Omega_{\rm out}$ is the outer domain of $\Omega_{\rm D}$ and is enclosed by $\Omega_{\rm PML}$ and $\Gamma_{\rm PEC}$.

We assume a transverse magnetic mode, $\mathbf{E} = [0,0,E_z]^T$, and solve the Helmholtz equation derived from Maxwell's equations as follows:

$$\nabla^2 E_{\rm s} + \frac{\omega^2}{c^2}\epsilon(\mathbf{x})E_{\rm s} = -\frac{\omega^2}{c^2}[\epsilon(\mathbf{x}) - \epsilon_{\rm air}]E_{\rm i},$$

where $E_{\rm s}$ and $E_{\rm i}$ denote the scattered and incident electric fields and satisfy $E_z = E_{\rm s} + E_{\rm i}$, ω denotes the circular frequency of light, and c the velocity of light in vacuum. With $\epsilon_{\rm air}$ and $\epsilon_{\rm dm}$ denoting the relative permittivities of air and dielectric material, respectively, the position-dependent relative permittivity $\epsilon(\mathbf{x})$ is defined as

$$\epsilon(\mathbf{x}) = \begin{cases} \epsilon_{\rm air} + \chi(\epsilon_{\rm dm} - \epsilon_{\rm air}) & \mathbf{x} \in \Omega_{\rm D}, \\ \epsilon_{\rm air} & \mathbf{x} \in \Omega_{\rm out}\,, \end{cases}$$

where χ is the characteristic function,

$$\chi(\phi(\mathbf{x})) = \begin{cases} 1 & \text{if } \mathbf{x} \in \Omega_{\rm dm}, \\ 0 & \text{if } \mathbf{x} \in \Omega_{\rm D}\backslash\Omega_{\rm dm}, \end{cases}$$

and $\phi(\mathbf{x})$ denotes a level-set function having piecewise-constant values [40,45] to the boundaries $\Gamma_{\rm dm}$ of the dielectric material such that

$$\begin{aligned} -1 \leqslant \phi(\mathbf{x}) < 0 \quad & \forall\, \mathbf{x} \in \Omega_{\rm D}\backslash\Omega_{\rm dm}, \\ \phi(\mathbf{x}) = 0 \quad & \forall\, \mathbf{x} \in \Gamma_{\rm dm}, \\ 0 < \phi(\mathbf{x}) \leqslant 1 \quad & \forall\, \mathbf{x} \in \Omega_{\rm dm}\backslash\Gamma_{\rm dm}. \end{aligned}$$

In designing the dielectric structures of carpet cloaks, the difference between the electric field reflected by a flat plane, $E_{\rm flat}$, and that controlled by a carpet cloak needs to be minimized. This determines the objective functional of the optimization defined as

$$\underset{\phi}{\text{minimize}} \quad F = \frac{1}{F_0}\int_{\Omega_{\rm out}} |E_{\rm flat} - E_z|^2 d\Omega, \tag{1}$$

where F_0, the normalization of F, is given as the integrated intensity of the difference between $E_{\rm flat}$ and the electric field when a bare bump exists, $E_{\rm bump}$. Specifically, we have

$$F_0 = \int_{\Omega_{\rm out}} |E_{\rm flat} - E_{\rm bump}|^2 d\Omega. \tag{2}$$

In general, topology optimization is an ill-posed problem and needs regularization. For this purpose we adopt the level-set method incorporating a fictitious interface energy [42], adding a corresponding energy term defined within the phase field model to the original objective functional F,

$$\underset{\phi}{\text{minimize}} \quad F_{\rm r} = F + \int_{\Omega_{\rm D}} \frac{1}{2}\tau|\nabla\phi|^2\, d\Omega, \tag{3}$$

where τ is the regularization parameter, which determines the ratio of the fictitious interface energy term to F. The above regularization is one of the perimeter controls, and we can obtain various optimal configurations with different structural profiles by adjusting the value of τ. As τ becomes smaller, confining the perimeter becomes weaker, implying that the performance of the optimally designed device is better.

The level-set function ϕ is updated by solving the time-evolution equation [42]

$$\frac{\partial\phi}{\partial t} = -\bar{F}' + \tau\nabla^2\phi, \tag{4}$$

where $\bar{F}'$ is the topological derivative derived from the conventional adjoint variable method [46] and derived as follows:

$$\bar{F}' = \text{Re}\left[-\frac{\omega^2}{c^2}(\epsilon_{\rm dm} - \epsilon_{\rm air})(E_{\rm s} + E_{\rm i})\tilde{E}\right], \tag{5}$$

where $\tilde{E}$ is the adjoint variable obtained from the adjoint equation [37,46].

III. RESULTS AND DISCUSSIONS

Figure 2 depicts the dielectric structures in $\Omega_{\rm D}$ and the scattered electric fields $E_{\rm s}$ for a flat plane, a bare bump, and an initial multilayer configuration. Incident plane waves are reflected by the flat PEC reflector; the scattered field is shown in Fig. 2(d). $P_{\rm N}$ represents the perimeter of the dielectric

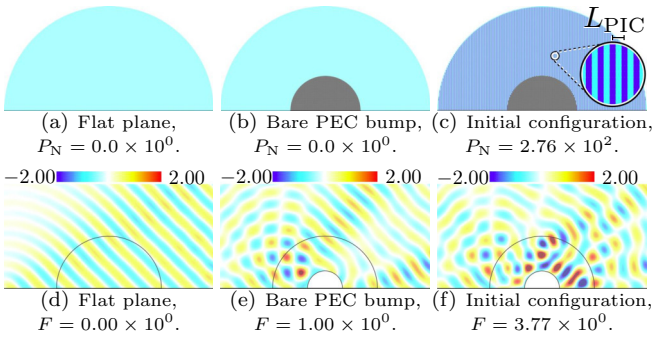

FIG. 2. Configurations and scattered field $\text{Re}\{E_{\rm s}\}/|E_{\rm i}|$ for a flat plane, bare PEC bump, and an initial multilayer configuration. The periodic length of the initial multilayer configuration is $L_{\rm PIC} = R_{\rm D}/100$. Relative permittivity is set to $\epsilon_{\rm dm} = 2.0$ (blue: dielectrics) and $\epsilon_{\rm air} = 1.0$ (cyan: air). The incident plane waves oscillate at $\omega R_{\rm D}/2\pi c = 2.5$.

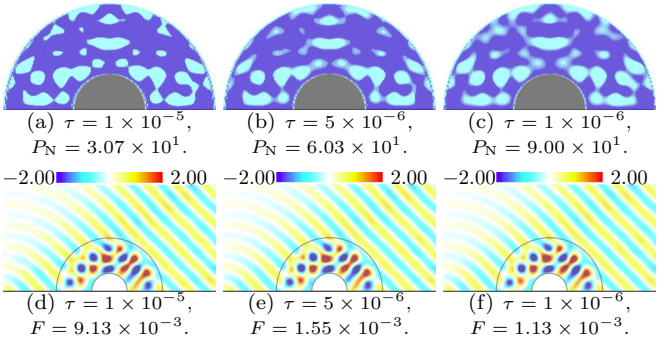

FIG. 3. (a)–(c) Optimal configurations obtained by each value of τ. Relative permittivity is set to $\epsilon_{dm} = 2.0$ (blue: dielectrics) and $\epsilon_{air} = 1.0$ (cyan: air). A semicircular black domain represents a semicylindrical PEC bump rendered invisible. (d)–(f) Scattered field, $\mathrm{Re}\{E_s\}/|E_i|$, when optimal configurations exist. The incident plane waves oscillate at $\omega R_D/2\pi c = 2.5$.

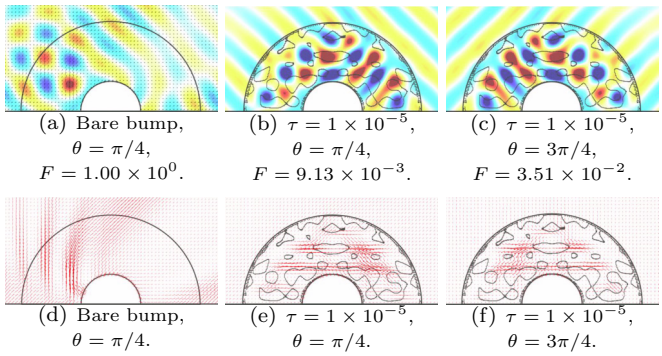

FIG. 4. Outline of the dielectric structure, the scattered field $\mathrm{Re}\{E_s\}/|E_i|$, and Poynting vector around the bump.

structure, and is computed as the summation of the lengths of edges between triangle elements of the dielectric and those of adjoining material. For a bare bump, as shown in Fig. 2(e), the incident waves are scattered in various directions with the bump being visible. The value of its objective functional becomes $F = 1$ through normalization using F_0 in Eq. (2). Figure 2(c) shows the initial configuration in regard to the present topology optimization. The design of carpet cloaks is a multimodal optimization problem and we cannot obtain optimal configurations having good cloaking performance except in optimizations starting from the initial configuration already presented. A multilayer arrangement along the x direction is set as the initial configuration for which the value of the objective functional becomes $F = 3.77$.

Figure 3 shows the optimal configurations and scattered field E_s of the optimal configuration for each value of τ. The τ values and the perimeter of the optimal dielectric structures P_N, normalized by R_D, are included with Figs. 3(a)–3(c), and the F of the optimal carpet cloak obtained for each τ are included with Figs. 3(d)–3(f). By comparing the fields in Ω_{out}, given in Figs. 3(d)–3(f) and those in Fig. 2(d), the optimally designed carpet cloaks imitate reflections from a flat reflector very well. As τ is set smaller in value, the corresponding F diminishes and the optimal configuration produces a larger perimeter P_N. Optimal configurations obtained with smaller τ, in particular $\tau = 1\times10^{-6}$, have multilayered dielectric structures that are considered to be the remains of the initial configuration. The weak confinement of the perimeter control allows the multilayered structures to remain, providing a large structural perimeter with the perimeter control implemented in Eq. (3) working as normal. The width of these remaining multilayered structures becomes the same as that of the initial configuration $L_{PIC} = R_D/100 = \lambda/40$ where λ is the wavelength of light in air. To realize these carpet cloaks operating at visible light of wavelength $\lambda = 580$ nm, the width L_{PIC} is estimated at 14.5 nm, which is the required tolerance for the fabrication of the optimal configuration obtained with $\tau = 1\times10^{-6}$.

Figure 4 shows the scattered fields and Poynting vectors of the fields around the bump. To avoid the scattering by the bump in Figs. 4(a) and 4(d), pores are created in the optimization process and scattered waves are trapped by resonance effects in the dielectric structure, as shown in Fig. 4(b). In Fig. 4(e), the Poynting vectors of the waves detour around the bump. The scattered waves are guided into the dielectric carpet cloak and emitted out at the same angle of reflection as that of a flat plane.

To reproduce reflections from a flat plane, the incident and scattered fields must satisfy time-reversal symmetry. Figures 4(c) and 4(f) show the scattered field and their Poynting vectors for an incident wave at $\theta = 3\pi/4$. The performance achieved was $F = 3.51\times10^{-2}$, meaning the value was sufficiently small; hence the optimal configuration functionally satisfies the time-reversal symmetry. When the carpet is cloaking perfectly, the incident wave should be reflected at the same angle of reflection as that of a flat plane. The time-reversal symmetry of the propagating field then certainly holds; hence the dielectric structure of the perfect carpet needs to have y-axis symmetry. The obtained optimal structures in Fig. 3 are not perfectly symmetric about the y axis because the optimal structures are determined subject to tradeoffs between minimizing F and minimizing the structural perimeter P_N. The structure of the carpet cloak is almost close to being symmetric during the optimization process. However, when conflict arises, the F value rises and the optimal structures obtained near minimum F become asymmetric about the y axis. When τ is set to zero, the conflict never occurs; however, to solve the ill-posed problem, τ must be nonzero to have any effect on controlling the perimeter. The grid size for the structural expression using level-set functions possibly becomes one of the causes of the structural asymmetry. Because of mesh-size dependencies in FE modeling, the grid size directly produces effects in computational accuracy for FE analysis, the calculation of topological derivatives, and evaluations of

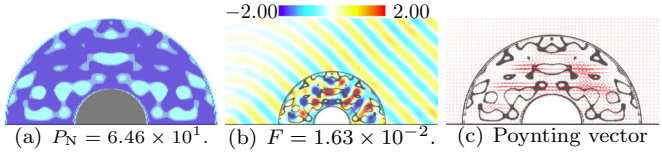

FIG. 5. Optimized results for $\tau = 1\times10^{-5}$ obtained by imposing the y-axis symmetry constraint on the level-set functions. (a) Optimal symmetric configuration. (b) Scattered field when a symmetric configuration is present. (c) Poynting vector of the scattered field.

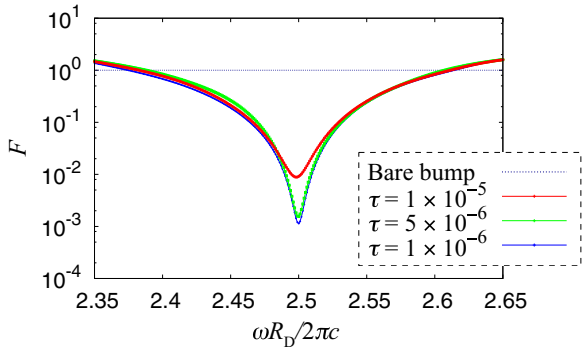

FIG. 6. Normalized frequency $\omega R_D/2\pi c$ versus objective functional value F. The incident angle is fixed at $\theta = \pi/4$.

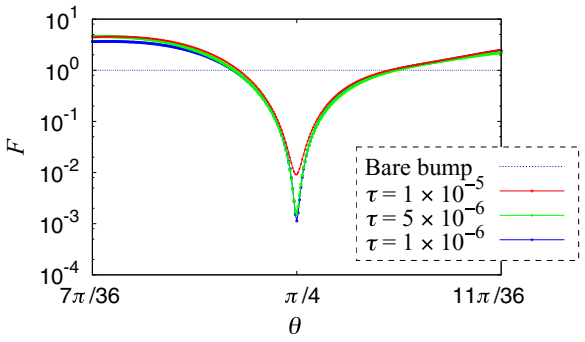

FIG. 7. Incident angle θ versus objective functional value F. The frequency is fixed at $\omega R_D/2\pi c = 2.5$.

the level-set functions. While a small grid size is desired, it must be determined subject to actual computational expense.

To investigate how much the cloaking performance can be improved by maintaining such structural symmetry, we designed an optimally configured carpet cloak subject to the y-axis symmetry constraint imposed on the level-set functions. Figure 5 depicts this configuration obtained for $\tau = 1\times10^{-5}$ along with its scattered field and Poynting vectors. Regardless of the structural symmetry requirements for perfect carpet cloaking, the performance of this carpet cloak with y-axis symmetry imposed ($F = 1.63\times10^{-2}$) is inferior to that of the cloak designed without the constraint ($F = 9.13\times10^{-3}$). The symmetry constraint about the y axis reduces the degrees of freedom in design and, as a result, worsens the performance of the optimal carpet cloak. To obtain desired optimal carpet cloaks, a compromise needs to be made between the performance, the structural complexity and symmetry, and the computational costs. When performance has priority over the exactness of the structural symmetry, optimizations without the constraint on the y-axis symmetry provide optimal configurations having better cloaking performances.

Figures 6 and 7 show the frequency and incident angle dependencies of F, respectively. The reflected field E_{flat} and the F_0 value in Eq. (2) need to be computed for every frequency and incident angle. When the center frequency of the visible light of 580 THz corresponds to $\omega R_D/2\pi c = 2.5$, the range $2.383 \leqslant \omega R_D/2\pi c \leqslant 2.611$ in which $F < 1$ for $\tau = 1\times10^{-5}$ corresponds to the visible frequency range $552.8 \leqslant f \leqslant 605.7$ THz. The dip frequency of $\tau = 1\times10^{-5}$ (Fig. 6) shifts a little lower than $\omega R_D/2\pi c = 2.5$. The shift is believed to arise because of the stronger confinement brought about by the larger value of τ. From a comparison between the results for $\tau = 5\times10^{-6}$ and 1×10^{-6}, no clear difference is perceived between their bandwidths at the frequency for invisibility.

IV. CONCLUSION

We introduced topology optimization for carpet cloaks made of dielectrics using a level-set boundary expression and optimized the structures of the carpet cloaks. The performance of these designed carpet cloaks at the target frequency is sufficient to realize invisibility and these carpet cloaks succeed at imitating reflections from a flat plane. Their performance and the perimeter of the optimal structures are controlled by adjusting the value of the regularization parameter τ. The design of carpet cloaks is a strong multimodal optimization problem, but we can find appropriate initial configurations leading to the optimal configurations having good performances. This topology optimization can produce various optimal configurations having quite different structural characteristics, and the symmetry of the configurations is satisfied approximately. These optimal carpet cloaks spontaneously satisfy the time-reversal symmetry of the scattered field during the optimization process.

ACKNOWLEDGMENT

This work was supported by JSPS KAKENHI Grant No. JP26870239.

[1] K. Ohtaka, Phys. Rev. B **19**, 5057 (1979).
[2] E. Yablonovitch, Phys. Rev. Lett. **58**, 2059 (1987).
[3] S. John, Phys. Rev. Lett. **58**, 2486 (1987).
[4] V. G. Veselago, Sov. Phys. Usp. **10**, 509 (1968).
[5] D. S. Wiersma, Nat. Photon. **7**, 188 (2013).
[6] G. Fujii, T. Matsumoto, T. Takahashi, and T. Ueta, Opt. Express **20**, 7300 (2012).
[7] T. Ueta, G. Fujii, G. Morimoto, K. Miyamoto, and A. Kosaku, Europhys. Lett. **107**, 34004 (2014).
[8] M. W. Takeda, S. Kirihara, Y. Miyamoto, K. Sakoda, and K. Honda, Phys. Rev. Lett. **92**, 093902 (2004).
[9] F. Miyamaru, S. Kubota, and M. W. Takeda, Appl. Phys. Express **5**, 072001 (2012).
[10] K. Edagawa, S. Kanoko, and M. Notomi, Phys. Rev. Lett. **100**, 013901 (2008).
[11] Z. V. Vardeny, A. Nahata, and A. Agrawal, Nat. Photon. **7**, 177 (2013).
[12] J. Li and J. B. Pendry, Phys. Rev. Lett. **101**, 203901 (2008).

[13] U. Leonhardt, Science **312**, 1777 (2006).
[14] J. B. Pendry, D. Schurig, and D. R. Smith, Science **312**, 1780 (2006).
[15] J. Valentine, J. Li, T. Zentgraf, G. Bartal, and X. Zhang, Nat. Mater. **8**, 568 (2009).
[16] M. Gharghi, C. Gladden, T. Zentgraf, Y. Liu, X. Yin, J. Valentine, and X. Zhang, Nano Lett. **11**, 2825 (2011).
[17] T. Ergin, N. Stenger, P. Brenner, J. B. Pendry, and M. Wegener, Science **328**, 337 (2010).
[18] B. Orazbayev, N. Mohammadi Estakhri, M. Beruete, and A. Alú, Phys. Rev. B **91**, 195444 (2015).
[19] X. Ni, Z. J. Wong, M. Mrejen, Y. Wang, and X. Zhang, Science **349**, 1310 (2015).
[20] M. P. Bendsøe and N. Kikuchi, Comput. Meth. Appl. Mech. Eng. **71**, 197 (1988).
[21] K. Suzuki and N. Kikuchi, Comput. Meth. Appl. Mech. Eng. **93**, 291 (1991).
[22] T. Yamada, K. Izui, and S. Nishiwaki, J. Mech. Des. **133**, 031011 (2011).
[23] K. Yaji, T. Yamada, M. Yoshino, T. Matsumoto, K. Izui, and S. Nishiwaki, J. Comput. Phys. **274**, 158 (2014).
[24] Y. Noguchi, T. Yamada, M. Otomori, K. Izui, and S. Nishiwaki, Appl. Phys. Lett. **107**, 221909 (2015).
[25] H. Men, K. Y. K. Lee, R. M. Freund, J. Peraire, and S. G. Johnson, Opt. Express **22**, 22632 (2014).
[26] W. R. Frei, H. T. Johnsona, and K. D. Choquette, J. Appl. Phys. **103**, 033102 (2008).
[27] W. R. Frei, H. T. Johnsona, and D. A. Tortorelli, Comput. Meth. Appl. Mech. Eng. **197**, 3410 (2008).
[28] D. C. Dobson and L. B. Simeonova, Appl. Math. Optim. **60**, 133 (2009).
[29] G. Fujii, T. Ueta, and M. Mizuno, Appl. Phys. A **116**, 921 (2014).
[30] L. H. Frandsen, A. H. Harpøth, P. I. Borel, M. Kristensen, J. S. Jensen, and O. Sigmund, Opt. Express **12**, 5916 (2004).
[31] M. Otomori, T. Yamada, K. Izui, S. Nishiwaki, and J. Andkjær, Comput. Meth. Appl. Mech. Eng. **237–240**, 192 (2012).
[32] J. Andkjær, N. A. Mortensen, and O. Sigmund, Appl. Phys. Lett. **100**, 101106 (2012).
[33] J. Andkjær and O. Sigmund, Appl. Phys. Lett. **98**, 021112 (2011).
[34] G. Fujii, H. Watanabe, T. Yamada, T. Ueta, and M. Mizuno, Appl. Phys. Lett. **102**, 251106 (2013).
[35] T. Yamada, H. Watanabe, G. Fujii, and T. Matsumoto, IEEE Trans. Magn. **49**, 2073 (2013).
[36] M. Otomori, T. Yamada, J. Andkjær, K. Izui, S. Nishiwaki, and N. Kogiso, IEEE Trans. Magn. **49**, 2081 (2013).
[37] G. Fujii, H. Watanabe, T. Yamada, T. Ueta, and M. Mizuno, in *Proceedings of the 10th World Congress on Structural and Multidisciplinary Optimization, WCSMO-10, Orlando, Florida, USA*, Paper 5283, 2013, http://www2.mae.ufl.edu/mdo/Papers/5283.pdf.
[38] L. Lan, F. Sun, Y. Liu, C. K. Ong, and Y. Ma, Appl. Phys. Lett. **103**, 121113 (2013).
[39] M. Selvanayagam and G. V. Eleftheriades, Phys. Rev. X **3**, 041011 (2013).
[40] P. Wei and M. Y. Wang, Int. J. Numer. Meth. Eng. **78**, 379 (2008).
[41] G. Fujii, T. Ueta, M. Mizuno, and M. Nakamura, Opt. Express **23**, 11312 (2015).
[42] T. Yamada, K. Izui, S. Nishiwaki, and A. Takezawa, Comput. Meth. Appl. Mech. Eng. **199**, 2876 (2010).
[43] J. P. Berenger, J. Comput. Phys. **114**, 185 (1994).
[44] A. Bermúdez, L. Hervella-Nieto, A. Prieto, and R. Rodríguez, J. Comput. Phys. **223**, 469 (2007).
[45] Z. Luo, L. Tong, J. Luo, P. Wei, and M. Y. Wang, J. Comput. Phys. **228**, 2643 (2009).
[46] R. M. Errico, Bull. Am. Meteorol. Soc. **78**, 2577 (1997).